Behavior of Elastomeric Seismic Isolators Varying Rubber Material and Pad Thickness: A Numerical Insight

Gabriele Milani[1] and Federico Milani[2]

[1] Politecnico di Milano, Piazza Leonardo da Vinci 32, 20133 Milan, Italy
[2] Chem.Co Consultant, Via J.F. Kennedy 2, 45030 Occhiobello (RO), Italy
gabriele.milani@polimi.it, federico-milani@libero.it

Abstract. A numerical approach for the determination of (a) the shear behavior under large displacements and (b) the compression elastic modulus of common parallelepiped elastomeric isolators is presented. Particular attention is devoted to the role played by the material used for the rubber pads and their thickness. For them, an experimental data fitting by means of both a nine constants Mooney-Rivlin and a five constants exponential law is utilized, within a Finite Element discretization of the isolator. Having at disposal a few experimental stretch-stress data points for each rubber compound in uniaxial tension, a cubic Bezier spline approach is firstly utilized, to generate numerically a large number of metadata containing the original experimental ones. Then, respectively the nine Mooney-Rivlin and five exponential law constitutive parameters are estimated through a least square approach. Once assessed the models, a full scale rectangular seismic isolator is analyzed when subjected to horizontal actions and normal compression, in order to provide estimates of the initial stiffness and the overall behavior of the isolator undergoing large deformations, using both models and for all the compounds considered. It is found that the global behavior may depend significantly on the material hypothesis assumed to model rubber and on pads thickness.

Keywords: Elastomeric Isolators, Rubber Typology, Compounds Performance, Stretch-strain Behavior under Large Deformations, Numerical Model Simulations, Finite Element Method, Pad Thickness.

1 Introduction

In the past, as a consequence of the high costs, elastomeric seismic isolation technology was very limited and mainly conceived for large, expensive buildings housing sensitive internal equipment, e.g. computer clusters, emergency operation centers, and hospitals. To extend this valuable earthquake-resistant strategy to common housing and commercial buildings, producers made several efforts to reduce the weight and cost of the isolators. Now they are available at relatively low prices, even for standard new buildings - Tsai & Lee [20], Hsiang-Chuan Tsai [9].

An elastomeric seismic isolator is a layered device constituted by thick rubber pads (10-30 mm) and thin reinforcing steel plates, laid between pads [13], see Fig. 1.

M.S. Obaidat et al. (eds.), *Simulation and Modeling Methodologies, Technologies and Applications*, Advances in Intelligent Systems and Computing 256,
DOI: 10.1007/978-3-319-03581-9_4,

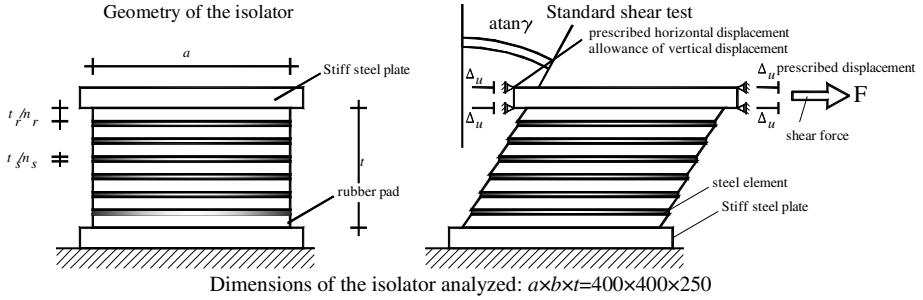

Fig. 1. Geometry of the elastomeric isolator

rubber pads may be realized with natural (NR) or artificial rubber (AR). NR is still the most diffused, but it will be superseded very soon in the built stock by AR, NR suffering from quick aging and being the industrial production capability limited. AR is usually neoprene, or less frequently, Braga et al. [4], EPDM (Ethylene Propylene Diene Monomer) and NBR-EPDM (Nitrile-Butadiene Rubber-EPDM) blend vulcanized with or without an increasing amount in weight of carbon black.

Thanks to rubber incompressibility [1,2] and the introduction of the thin steel sheets, a seismic isolator is extremely deformable for horizontal forces, but at the same time sufficiently stiff when loaded with vertical actions. This is essential in buildings subjected to seismic loads, where the main goal to achieve is to "isolate" (i.e. increase the period of the structure) the whole structure to the ground when seismic load acts and to sustain the vertical loads transferred to the foundation.

In this work, the influence of rubber pads mechanical properties and thickness on both vertical and horizontal stiffness of realistic seismic isolators is discussed. A number of different rubber blends available in the market are considered, to show that a different performance is achieved at a structural level when different materials for the pads are used. A numerical approach based on experimental data fitting is adopted to characterize the mechanical behaviour under tensile stretching and pure shear. Both a nine constants Mooney-Rivlin model [14] and an exponential law [1,2] are assumed for the evaluation of the energy density. Constants entering in both models are estimated by means of a standard least squares routine fitting experimental data available. Due to the insufficient number of experimental values at disposal, Bezier splines are utilized to numerically generate a large number of (meta)data.

Once that the unknown coefficients are evaluated for both models and for all the compounds analyzed, a standard parallelepiped seismic isolator is simulated using FEs in compression and in pure shear tests under large deformation. To perform the simulations, both a Mooney Rivlin and an Amin et al. [1] model, see also Milani & Milani [11,12] are implemented in an existing non commercial large deformation FE code.

Having at disposal an idealized mechanical behaviour for the pads to be used at a structural level, a second parameter that may influence the overall behaviour of the devices is investigated, namely the thickness of the single pads, Milani & Milani [12], which may vary the overall elastic compression modulus E_c of the isolator. E_c is evaluated by means of a full 3D Finite Element discretization, comparing results

obtained with the model proposed with those provided by [19] model and Italian code [15] formulas, varying both first shape factor in the range of technical interest and compound used in the rubber pad.

From simulations results, generally, it is found that the most indicated compound is neoprene heavily loaded with C/B (Carbon Black), or an EPDM and NBR-EPDM blend with C/B in variable weight percentage. Both of them suffer from a sudden increase of the stiffness at relatively high stretches, meaning that a non-linear analysis of the building should be performed in this case.

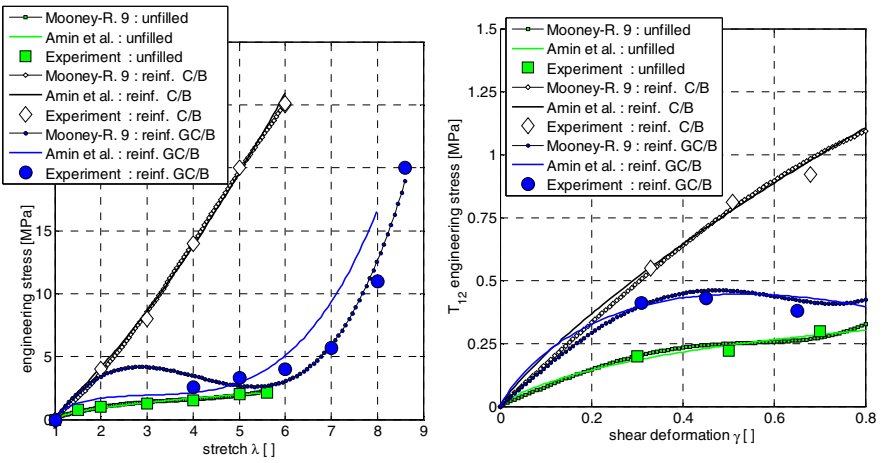

(a) (b)

Fig. 2. Unfilled, reinforced with carbon black (C/B) and with graphitized carbon black (GC/B) generic non crystallized rubber. –a: Uniaxial stretch-nominal stress diagram. –b: simple shear behaviour. Experimental data and numerical (Mooney Rivlin and 5 constants [1]) models response.

2 Pads Uniaxial and Shear Experimental Behavior at Finite Deformations with Different Materials

The most commonly performed mechanical test to charaterize rubber vulcanizates is the uniaxial extension of a strip to its breaking point. Fig. 2-a shows schematically the uniaxial stretch-stress behavior of an amorphous rubber incapable of crystallization under strain. The first curve (with green squares) is for a gum vulcanizate, the second (white diamonds) for a vulcanizate reinforced with a high-surface-area structure carbon black (C/B), and the latter for a vulcanizate reinforced with the same black after graphitization (GC/B). As it can be noticed, sample with C/B exhibits an initial slope of the stretch-strain curve much greater, typically due to the contribution of the filler. Such increase in initial stiffness varies varying the amount and typology of the filler and is a function of the state of subdivision of the filler and hence of its specific surface area. Once the effects of secondary agglomeration are overcome, several mechanisms remain, responsible of the stress rising faster than in the unfilled sample:

the most important is the strain amplification, since the rigid filler does not share in the deformation, Bueche [6]. It is clear that the inclusion of a rigid adhering filler in a soft matrix will cause the average local strain in the matrix to exceed the macroscopic strain. As a consequence, the rubber in the filled vulcanizate is highly strained and responds with a higher stress. Strain amplification also increases the mean rate at which the matrix is strained, leading to a further increase in stress.

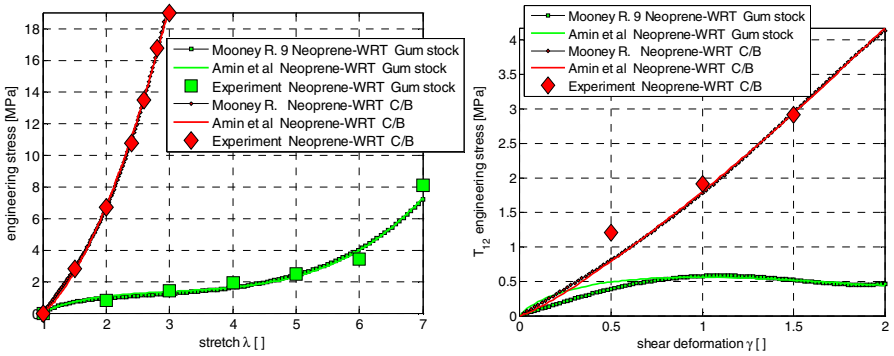

Fig. 3. Neoprene WRT with C/B and Gum stock. –a: Uniaxial stretch-nominal stress diagram. –b: simple shear behaviour. Experimental data and numerical (Mooney Rivlin and 5 constants [1]) models response.

Stretch-stress data reported in Fig. 3-a are post-processed from experimental data collected in Studebaker & Beatty [17] and represent the typical uniaxial behavior of neoprene gum stock in comparison with neoprene loaded with carbon black at 50 phr. In general, in this case the behavior of the neoprene sample loaded with carbon black is sensibly stiffer, with a rather marked increase of the tensile strength and a decrease of elongation at break, which is typical of loaded elastomers.

Similar considerations may be repeated for shear tests, Fig. 3-b. Shear initial stiffness may depend strongly on the cristallization degree and on the amount of filler and unsaturation. However, to have at disposal shear experimental data is not always possible, see Fig. 2-b. When available, numerical models coefficients are obtained by least squares on all experimental data.

In Fig. 4-a, the uniaxial stretch-stress behavior of unfilled and filled EPDM is represented. Data are kept from Studebaker & Beatty [17]-. Here, it is worth noting that the filler amount used is exactly the same used for neoprene in Fig. 3. Tensile strength increases using carbon black, but, differently to neoprene, the elongation at break is almost the same of the unfilled compound, passing from 4.2 to 5.1: this is due to the low unsaturation of the EPDM rubber when compared with neoprene, natural rubber etc. Conversely, tensile strength is comparable to neoprene. Therefore, one of the advantages of EPDM compared with neoprene would be the more ductile behavior.

In Fig. 5-a, a comparison between stretch-stress curves for neoprene and a mixture of nitrile rubber (Elaprim-S354-EP) and EPDM (Dutral TER 9046) in the ratio of

70:30 in weight is represented for a standard tensile stress experimentation. Two experimental curves for Elaprim+Dutral are reported, to show the low experimental data scattering. The vulcanization conditions are nearly the same (160° for 30 and 20 minutes for neoprene and Elaprim+Dutral respectively). Both rubber compounds have been loaded with carbon black at 50 phr.

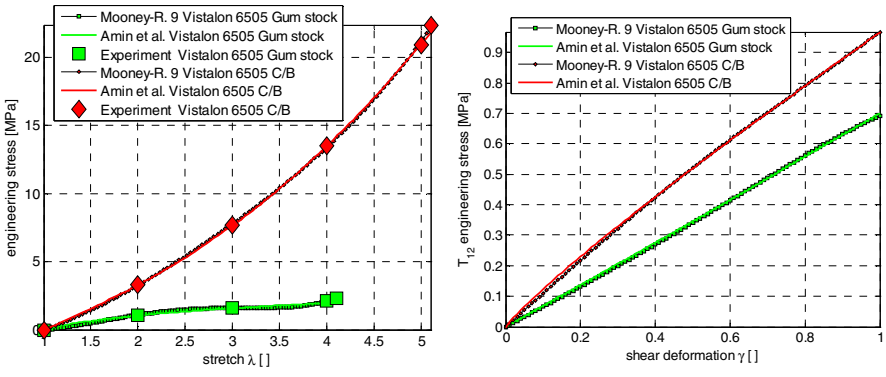

Fig. 4. EPDM Vistalon 6505 Gum stock and Vistalon 6505 with C/B. –a: Uniaxial stretch-nominal stress diagram. –b: simple shear behaviour. Experimental data and numerical (Mooney Rivlin and 5 constants [1]) models response.

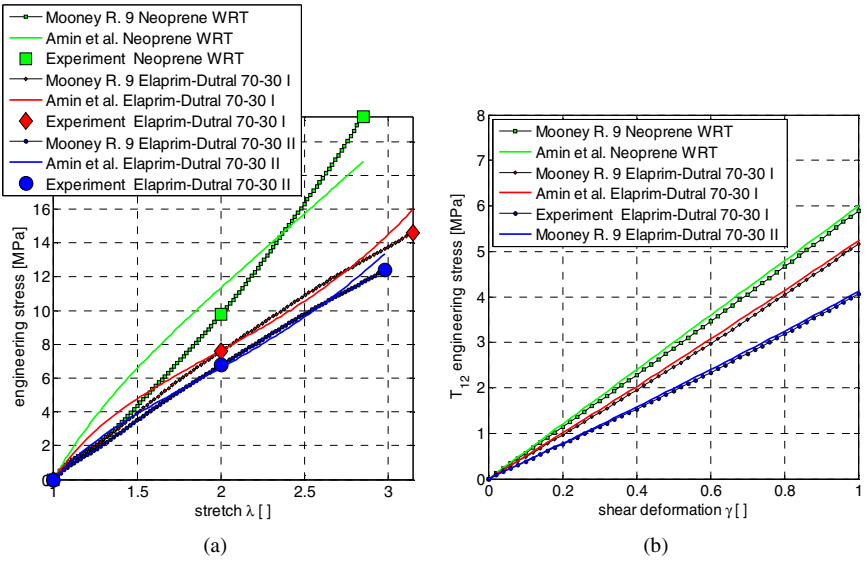

Fig. 5. Neoprene WRT, Elaprim-Dutral 70-30 (1st test) and Elaprim-Dutral 70-30 (2nd test) compounds. –a: Uniaxial stretch-nominal stress diagram. –b: simple shear behaviour. Experimental data and numerical (Mooney Rivlin and 5 constants [1]) models response.

Neoprene behavior is nearly linear, with slightly higher tensile strength. The elongation at failure is comparable for both compounds. While generally it can be stated that neoprene mechanical performance is preferable, mainly for its quite linear response even at high levels of stretches, it is worth mentioning that nitrile rubber added with EPDM has some other advantages, as for instance the lower cost, lower time of vulcanization, lower specific weight for the items. In any case, limiting the analyses for stretches under 2 or shear distortion angles lower than 45°, Fig. 5-b, the mechanical behavior is, from an engineering point of view, the same, meaning that if a seismic isolator is designed to undergo deformations where rubber pads do not exceed this threshold stretch, nitrile rubber and EPDM may be considered as a valid alternative to neoprene.

3 Numerical Model for Rubber Pads: Nine Constants Mooney Rivlin and Amin et al. [1,2] Exponential Model

In an uniaxial test, we usually define the stretch as the ratio between the length in the deformed configuration divided by the length in the undeformed state. Let $\lambda_1 = \lambda$ be the stretch in the direction of elongation and $\sigma_1 = \sigma$ the corresponding stress. The other two principal stresses are zero, since no lateral forces are applied $\sigma_2 = \sigma_3 = 0$. For constancy of volume, the incompressibility condition $\lambda_1\lambda_2\lambda_3 = 1$ gives $\lambda_2 = \lambda_3 = 1/\sqrt{\lambda}$. The strain energy function, in the most general case, for the Mooney-Rivlin model is given by:

$$W = \sum_{r=0\,s=0}^{m,n} C_{rs}\left(I_1 - 3\right)^r \left(I_2 - 3\right)^s \quad C_{00} = 0 \tag{1}$$

where $I_1 = \lambda_1^2 + \lambda_2^2 + \lambda_3^2$ and $I_2 = \lambda_1^{-2} + \lambda_2^{-2} + \lambda_3^{-2}$.

When dealing with the six constants Amin et al. (2006) model, the strain energy function is given by:

$$W = C_2\left(I_2 - 3\right) + C_5\left(I_1 - 3\right) + \frac{C_3}{N+1}\left(I_1 - 3\right)^{N+1} + \frac{C_4}{M+1}\left(I_1 - 3\right)^{N+1} \tag{2}$$

where C_2, C_3, C_4, C_5, N, M are material parameters to be determined. Amin et al. [1] five constants model is obtained simply assuming C_2=0.

In uniaxial tension or compression equations it can be shown that the strain invariants are $I_1 = \lambda^2 + 2\lambda^{-1}$ and $I_2 = 2\lambda + \lambda^{-2}$. The engineering stress S' (force per unit unstrained area of cross-section) may be evaluated from energy density as follows:

$$S' = 2\left(1 - \frac{1}{\lambda^3}\right)\left(\lambda\frac{\partial W}{\partial I_1} + \frac{\partial W}{\partial I_2}\right) \tag{3}$$

To fully characterize a rubber compound in terms of Mooney-Rivlin stress-stretch curves, it is therefore necessary to perform suitable experimental mono-axial tests in pure traction and/or shear at large deformations on different rubber compounds. The relationship between the nominal stress and the corresponding stretch, after substituting the corresponding strain energy density function (1) or (2) into (3) can be generalized as follows:

$$S'(\lambda) = S'(C_k, \lambda) \tag{4}$$

where C_k are material constants in the strain energy density function, see Fig. 6-a. Equation (4) holds also in presence of experimental data available for pure shear tests, i.e. $T_{12}(\gamma) = T_{12}(C_k, \gamma)$, where γ identifies the shear strain, namely the distortion of

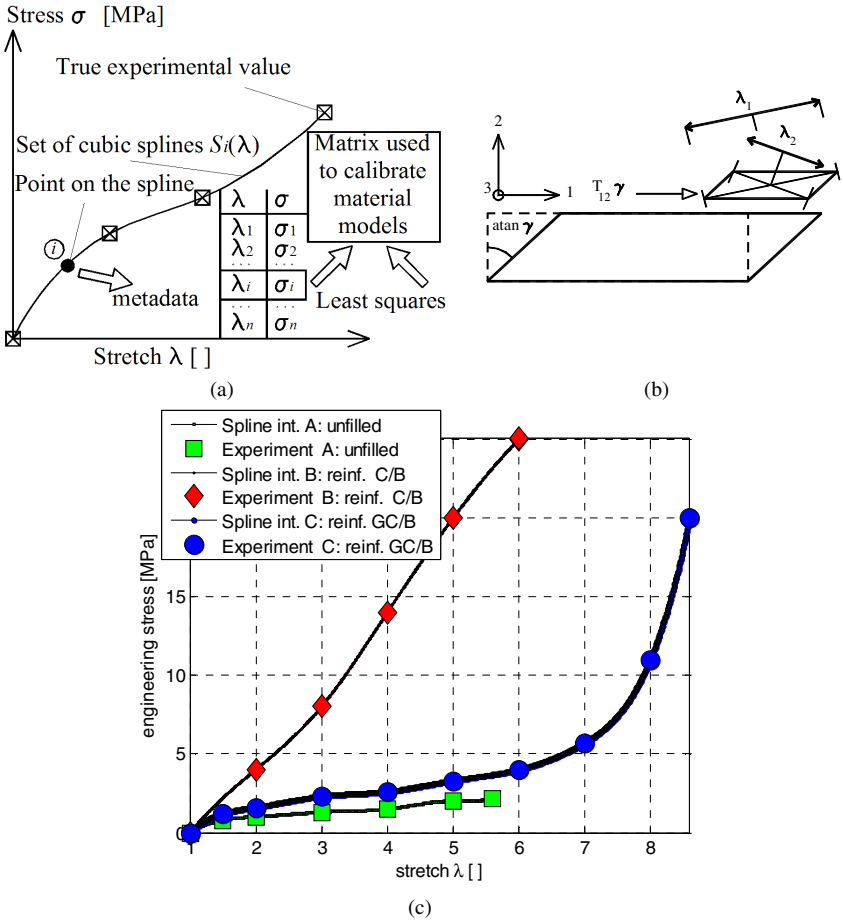

Fig. 6. Numerical procedure adopted to fit experimental data and to calibrate the material parameters model. -a: fitting of experimental data (squares) by means of a set of natural cubic splines and subsequent metadata extraction to use as input points to calibrate the material constants through least squares. –b: pure shear deformation: principal stretch directions, shear angle and T12 shear internal action. -c: splines fitting for the compounds represented in Fig. 2.

a rectangle subjected to pure shear, Fig. 6-b. C_k are determined by a (non) linear least squares fitting performed on experimental data and equation (4).

Assuming that there are $\overline{N}\left(\overline{N} \geq \overline{M}\right)$ pairs of experimental data (nominal stress and stretch, say $\overline{S}_i$ and $\overline{\lambda}_i$), we minimized the sum of squared differences between the calculated and the measured stress values, i.e.:

$$\min\left\{\sum_{s=1}^{N}\left(\overline{S}'_i - S'\left(\overline{\lambda}_i\right)\right)^2\right\} \tag{5}$$

Equation (5) differentiated with respect to C_k variables leads to a system of linear (in the Mooney Rivlin case) equations:

$$\sum_{s=1}^{N}\left(\overline{S}' - S'\left(\overline{\lambda}\right)\right)\left.\frac{\partial S'}{\partial C_k}\right|_{\lambda=\overline{\lambda}} = 0 \quad k = 1,\ 2,\ \overline{M} \tag{6}$$

which permits an evaluation of C_k constants. However, experimental data are usually insufficient ($\overline{N} \leq \overline{M}$) and therefore a numerical fitting is needed to collect (meta) data, which are assumed as reasonable approximation of experimental evidences. In order to avoid a polynomial fitting model, which is not unique and with an insufficient fitting performance, the actual experimental curve is approximated using a set of Bezier cubic splines and, subsequently, several intermediate points between the actual experimental data are numerically evaluated on the spline, to be used within a least squares procedure for material data calibration.

In pure shear deformation, see Fig. 6-b, and differently to uniaxial compression, the direction of applied displacement does not coincide with the direction of principal stretches; rather it involves a rotation of axes. Due to applied shear strain γ, the deformation gradient tensor $\mathbf{F}$ and the left Cauchy-Green deformation tensor $\mathbf{B}$ are described as:

$$\mathbf{F} = \begin{bmatrix} 1 & \gamma & 0 \\ 0 & 1 & 0 \\ 0 & 0 & 1 \end{bmatrix} \qquad \mathbf{B} = \begin{bmatrix} 1+\gamma^2 & \gamma & 0 \\ \gamma & 1 & 0 \\ 0 & 0 & 1 \end{bmatrix} \tag{7}$$

Consequently, the strain invariants are expressed as $I_1 = I_2 = 3 + \gamma^2$, $I_3 = 1$ and the expression for Cauchy stress becomes:

$$T_{12} = 2\gamma[\partial W / \partial I_1 + \partial W / \partial I_2] \tag{8}$$

The principal stretches associated with shear strain γ may be obtained as:

$$\lambda_1 = \sqrt{1 + \frac{\gamma^2}{2} + \gamma\sqrt{1 + \frac{\gamma^2}{4}}} \qquad \lambda_2 = \sqrt{1 + \frac{\gamma^2}{2} - \gamma\sqrt{1 + \frac{\gamma^2}{4}}} \tag{9}$$

λ_1 represents the principal tension stretch whereas λ_2 represents the principal compression stretch.

The shear stress in the six constants Amin et al. model (2006) is, for pure shear deformation, the following:

$$T_{12} = 2\gamma\left[C_5 + C_2 + C_4\gamma^{2M} + C_3\gamma^{2N}\right] \tag{10}$$

which reduces to $T_{12} = 2\gamma\left[C_5 + C_4\gamma^{2M} + C_3\gamma^{2N}\right]$ in the five constants model by Amin [1].

Where shear test data are available, parameters are obtained using a least squares routine on both tensile and shear tests experimental data, as envisaged in Amin et al. [2]. In absence of shear experimental data, parameters are evaluated only on the uniaxial behavior of the specimens. Resultant shear stress-deformation curves by Mooney-Rivlin and Amin et al. [1] models are in any case compared, to show how different is the response of the models when the fitting procedure is performed only on uniaxial tests.

In Fig. 6-c, for instance, the interpolation obtained with a cubic spline on experimental data of Fig. 2 is shown. As it is possible to notice, the fitting is almost perfect and allows to collect a number of 'metadata', which are defined hereafter as numerical stretch-stress points to use to calibrate rubber material properties and, in practice, will be used as they were a large set of experimental data available. This procedure is obviously necessary if a material model with many parameters has to be calibrated.

In figures from Fig. 2 to Fig. 5 a comparison among experimental mono-dimensional data (both tensile stress and shear) and curves provided by the two numerical models (nine constants Mooney-Rivlin and five constants [1] model) is represented. As expected, generally, the mono-axial behavior of polymers is well fitted by both models. On the other hand, shear behavior provided by both models is comparable and, in some cases, almost identical.

4 Influence of Pads Thickness on Elastic Compression Modulus

To evaluate the elastic compression modulus of a seismic isolator, a FE discretization is recommended. Due to the high vertical stiffness, linear elastic analyses are sufficient to determine precisely the compression modulus. Under small deformations rubbers are linearly elastic solids. Because of the high modulus of bulk compression, about 2000MN/m^2, compared to the shear modulus G, about 0,2-5MN/m^2 [18], they may be regarded as relatively incompressible. The elastic behavior under small strains can thus be described by a single elastic constant G, being Poisson's ratio very near to ½ and Young's modulus E equal to 3G with very good approximation.

In any case, elastic parameters to assign to single pads should be known in advance. In general, the so-called static modulus of a rubber compound is obtained in a standard stress-strain test in which the samples are extended at the rate of 20 in/min.

Hardness measures may help in the estimation of the elastic modulus, when a standard stress-strain characterization is not possible, takes too much time or it is too expensive. The test method ASTM D2240 [3] helps in the definition of a standard for

hardness evaluation, standardizing the penetration of a specified indentor forced into the material under specified conditions.

In order to have the possibility to evaluated the relationship between hardness and Young's modulus, a semi empirical relation between the shore hardness and Young's modulus for elastomers has been derived by Gent (1978). This relation has the following form:

$$E = \frac{0.0981(56 + 7.62336 S_H)}{0.137505(254 - 2.54 S_H)} \tag{11}$$

where E is the Young's modulus in MPa and S is the shore hardness. This relation gives a value of E equal to infinite at S_H=100, but departs from experimental data for S_H lower than 40.

Another relation that fits experimental data slightly better is the following and is reported into British standards (BS 1950, BS 1957):

$$S_H = 100 erf\left(3.186 \times 10^{-4} \sqrt{E}\right) \tag{12}$$

where erf is the error function and E is in units of Pa. A first order estimate of the relation between shore D hardness and the elastic modulus for a conical indenter with a 15 degree cone is:

$$S_D = 100 - \left[20\left(-78.188 + \sqrt{6113.36 + 781.88E}\right)\right] / E \tag{13}$$

where S_D is the shore D hardness and E is in MPa.

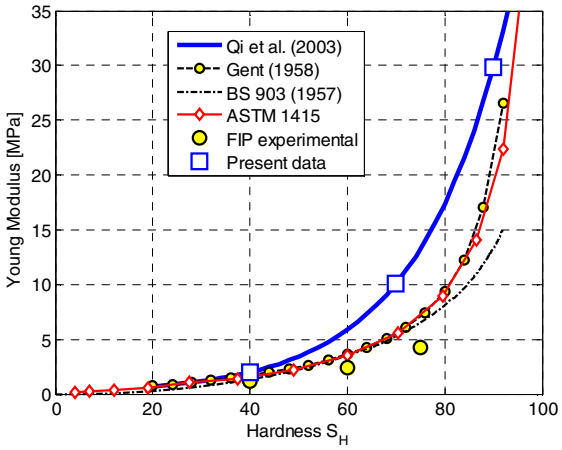

Fig. 7. Empirical dependence of the rubber elastic modulus in terms of international hardness. Squares denote elastic moduli used in the numerical simulations.

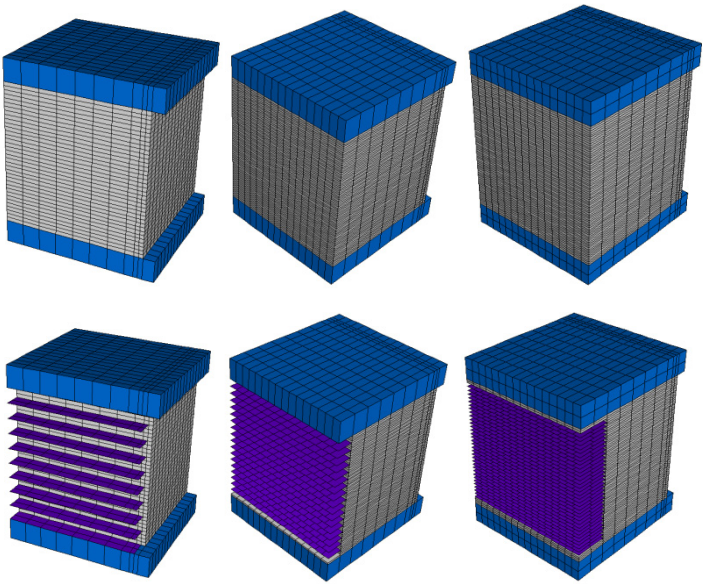

Fig. 8. FE discretization of the seismic isolators studied

A further recent linear relation between the shore hardness and the natural logarithm of Young's modulus is applicable over a large range of shore A and shore D hardness (Q_i , H) [16]. This relation has the form:

$$\ln(E) = 0.0235S_H - 0.6403 \tag{14}$$

where S_H=S_A for S_A between 20 and 80 and S_H=S_D +50 for S_D between 30 and 85, being S_A the shore A hardness, S_D the shore D hardness and E the Young's modulus in MPa.

Having at disposal hardness-Young modulus relationships of Fig. 7, they can be used in the FE model for the characterization of Ec compression modulus of the isolator.

The seismic isolator under study is a typical rectangular device which may be found in common building practice, Kelly [10], De Luca & Imbimbo [7], etc. The bearing, see Fig. 1 for the geometric dimensions, is composed by two steel plates, each 20 mm thick, between which rubber-steel elastomer are placed. One of the key parameters having a fundamental role in the determination of overall isolator compression elastic modulus E_c is the so called shape factor S (or primary shape factor), defined as the ratio between the loaded area and the lateral surface free to bulge. Since the shape factor refers to the single rubber layer, it represents a measure of the local slenderness of the elastomeric bearing. Experimental tests have shown that low shape factor bearings, characterized by values of S greater than 5 and less than 20, provide an isolation effect in both the horizontal and vertical directions whereas high shape factor bearings, characterized by values of S greater than 20, only provide a good isolation in the horizontal direction. It is even obvious that low values of the shape factor define thick rubber layers and, hence, provide bearings

characterized by high deformability. As a rule, in seismic isolation applications the need to have a device with a high vertical stiffness and low shear stiffness requires that S assumes values greater than 5 and less than 30. The Finite Element model shown in Fig. 8 is used to model ¼ of the bearing subjected to compression. Three geometric cases corresponding to shape factors S around equal to 7, 15 and 30 are hereafter considered. In these cases, the thicknesses of the single pad are respectively equal to 15, 22.5 and 45 mm. Assuming in the first case a thickness of steel laminas equal to 1 mm, in the second 2 mm and in the third 3 mm, the number of steel plates to be used on such devices is respectively equal to 14, 10 and 5. Two types of elements are utilized, namely 8 noded plate and shell elements for thin laminas, and 20 nodes brick elements for the hyper-elastic material (rubber). For steel laminas, an isotropic elastic behavior has been assumed. Following literature data, we adopted a Young Modulus E = $2x10^5$ MPa with Poisson ratio ν = 0.3. For a shape factor S equal to 7 the number of rubber pads is 9 (2 pads with ½ thickness at the top and bottom), for S=15 is 18 and for S=30 is 36.

In Fig. 9-a, the trend of the initial compression elastic modulus E_c provided by the present FE approach is compared with those evaluated by means of the Tsai and Kelly [19] model and by the Italian code [15]. Deformed shapes of the bearings in pure compression are also represented. When dealing with the Italian code, E_c is evaluated as $E_c = \left(1/6G_{din}S^2 + 4/3E_b\right)^{-1}$, where G_{din} is the dynamic shear modulus of the isolator (hereafter assumed equal to rubber shear modulus in absence of experimental data available) and E_b is the rubber bulk modulus (hereafter assumed infinite, being rubber almost incompressible). For the sake of conciseness, only three different rubber compounds are tested, namely a Neoprene and an EPDM tested in pure tension by the authors [11] and a commercial Neoprene (DuPont) used ordinarily for seismic isolation. As it is possible to notice from the figure, a very good agreement is found between present FE results and Tsai & Kelly [19] model. Evident but in any case acceptable differences may be noticed for high shape factors between present model and Italian code predictions. However, here it is worth noting that data assumed for shear and bulk moduli are rather questionable and may strongly affect output

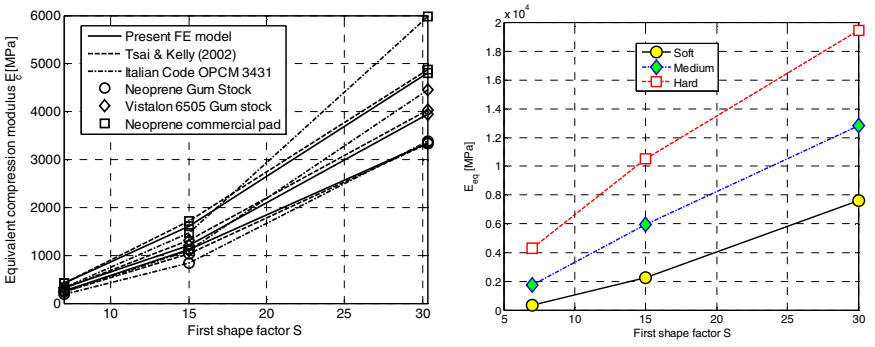

(a) (b)

Fig. 9. Isolator vertical elastic modulus varying shape factor and rubber hardness

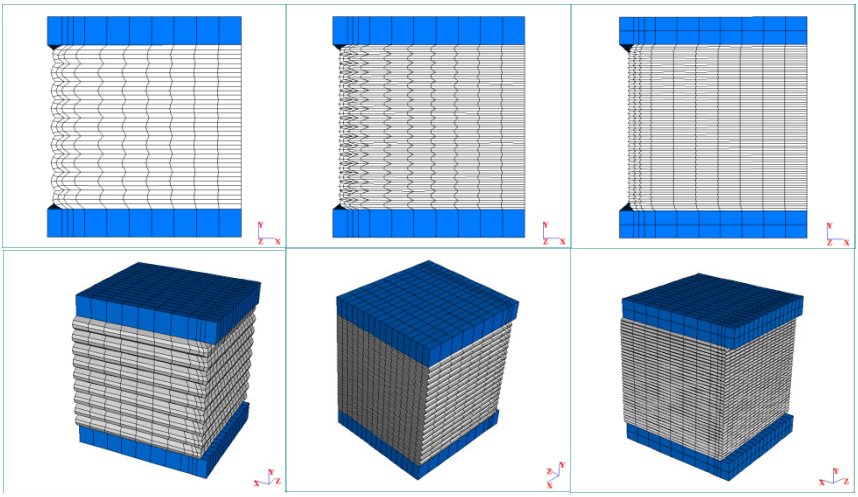

Fig. 10. Deformed shapes for vertical compression

numerical data for S>20. Finally, additional elastic analyses under small deformations are performed to characterize the vertical elastic modulus in compression at different values of the shape factor and for the three blends represented in Fig. 7 with square symbols, roughly corresponding to soft, medium and hard rubber.

As expected, elastic modulus increases with shape factor and is maximum for the hard blend. Usually, elastic moduli of a seismic isolator should range between 1500 and 7500 MPa, meaning that for a shape factor equal to 15, a medium or a soft blend should be used. Conversely, for higher shape factor, soft blend could have the beneficial role to progressively decrease vertical stiffness, whereas for lower shape factors hard blends are preferable.

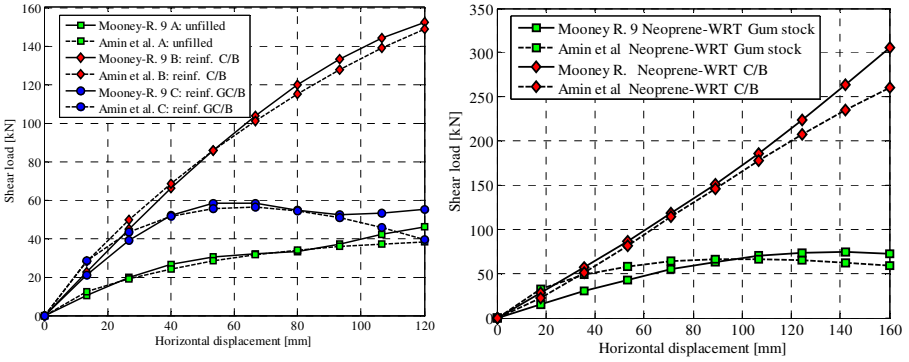

(a) (b)

Fig. 11. -a: Unfilled, reinforced with carbon black (C/B) and with graphitized carbon black (GC/B) generic non crystallized rubber. –b: EPDM Vistalon 6505 Gum stock and Vistalon 6505 with C/B. Seismic isolator global behavior under shear loads (total shear vs horizontal displacement curves obtained with a 9 constants Mooney Rivlin model and a 5 constants exponential model).

5 Shear Behavior of the Isolator

Lateral force (shear)-horizontal displacement behavior is predicted by means of the models previously described, at high levels of horizontal displacement. Clearly, for severe deformations, a large displacement analysis is required, under the hypothesis of modeling rubber through both a 9 constants Mooney-Rivlin and a 5 constants exponential model. Material constants are obtained using the procedure described in the previous Section.

Since the model proposed by Amin et al. [1] normally is not available in commercial codes, a Matlab based Open FEM software has been modified in order to implement an exponential law for the strain energy density function. The code obviously allows the usage of both brick and shell elements in large deformations.

In the model, a generic rubber (Fig. 2) and the neoprene with uniaxial behavior represented in Fig. 3 (filled with C/B) are considered, assuming the vertical displacement at the top edge of the stiff steel plate of the isolator not allowed. Since the global response of the isolator in terms of deformed shape is very similar in all the cases analyzed, a small sample of the huge amount of numerical results obtained are hereafter reported for the sake of conciseness. In particular, results in terms of applied shear at the top edge and corresponding horizontal displacement (which indirectly define the shear stiffness of the isolator) are depicted in Fig. 11 for the generic rubber (-a) of Fig. 2 and the neoprene (-b) of Fig. 3. As a rule, Mooney Rivlin and Amin et al. [1] models behave globally and generally in a similar way, providing comparable levels of horizontal load at assigned deformation.

This notwithstanding, it is worth noting that, in general, when hyperelastic constants are deduced exclusively from uniaxial tests fitting, some remarkable differences in shear tests between the models are possible. In addition, it is worth emphasizing that, in the case here analyzed, rubber pads are subjected to a complex state of stress depending on several factors, comprising the bending stiffness of the steel elements, the vertical pre-compression, etc., thus complicating further the prediction of their actual behavior.

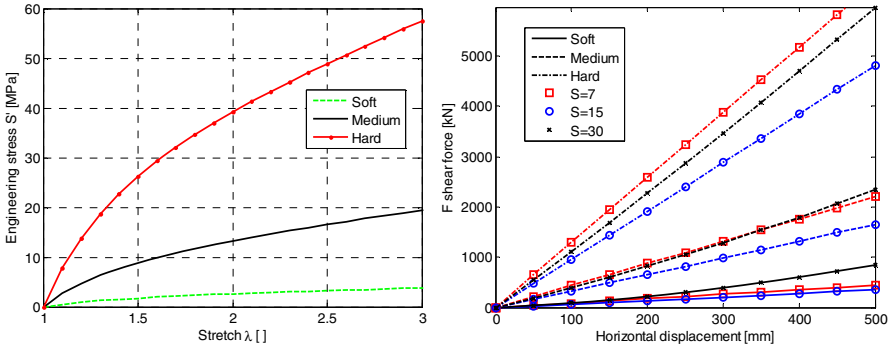

(a) (b)

Fig. 12. Stretch-stress behaviour of a single rubber pad (left) and pure shear behaviour under large deformations (right) of a square isolator.

To study the shear behavior of the isolator as a function of rubber pads hardness, a two constants Mooney-Rivlin model is utilized, in order to put at disposal to practitioners a simple FE model that can be implemented in any FE commercial code.

The uniaxial stress-stretch behavior of the 2 constants Mooney-Rivlin model adopted to evaluate the shear behavior of a single pad in presence of soft, medium and hard rubber is depicted in Fig. 12-a. The resultant shear force F-horizontal displacement of the entire isolator is represented in Fig. 12-b. Such representation may be particularly useful for practical purposes, since such curves may be implemented at a structural level to study entire base-isolated buildings in the dynamic range. As it is possible to notice, the utilization of different hardness rubber pads in conjunction with slender or less slender isolators may considerably change the macroscopic response of the isolator and, hence, the effectiveness of the device inserted in a large case structure may be variable.

6 Conclusions

The important matter of the role played by the material used and the thickness of rubber pads within seismic isolators has been investigated by means of a comprehensive FE set of analyses in linear elasticity and large deformations. From the results obtained, it can be deduced that a proper calculation is needed when the seismic isolator is constituted by pads with large thickness. Hardness is finally a very practical key parameter to define rubber initial Young's modulus, whereas full stretch-stress uniaxial curves are needed within refined numerical models to describe rubber behavior under large deformations.

References

1. Amin, A.F.M.S., Alam, M.S., Okui, Y.: An improved hyperelasticity relation in modeling viscoelasticity response of natural and high damping rubbers in compression: experiments, parameter identification, and numerical verification. Mech. Mater. 34, 75–95 (2002)
2. Amin, A.F.M.S., Wiraguna, I., Bhuiyan, A.R., Okui, Y.: Hyperelasticity Model for Finite Element Analysis of Natural and High Damping Rubbers in Compression and Shear. Journal of Engineering Mechanics ASCE 132(1), 54–64 (2006)
3. ASTM D2240-91. Standard test method for fubber property- Durometer hardness. Annual book of ASTM standard, 388–391 (1992)
4. Braga, F., Dolce, M., Ferrigno, A., Laterza, M., Marotta, G., Masi, A., Nigro, D., Ponzo, F.: Development of new materials for seismic isolation and passive energy dissipation - part i: experimental tests on new compound elastomeric bearings. In: Proc. International Post-SMiRT Conference Seminar on Seismic Isolation, Passive Energy Dissipation and Active Control of Seismic Vibrations of Structures Taormina, Italy (1997)
5. British Standard 903 (1950, 1957). Methods of testing vulcanized rubber, Part 19 (1950) and Part A7 (1957)
6. Bueche, F.: Mullins effect and rubber-filler interaction. Journal of Applied Polymer Science 5(15), 271–281 (1961)
7. De Luca, A., Imbimbo, M.: F. E. stress analysis of rubber bearings under axial loads. Computers and Structures 68, 31–39 (1998)

8. Gent, A.N.: Rubber elasticity: basic concepts and behavior. In: Eirich, F.R. (ed.) Science and Technology Rubber. Academic Press, NY (1978)
9. Tsai, H.-C.: Compression analysis of rectangular elastic layers bonded between rigid plates. International Journal of Solids and Structures 42(11-12), 3395–3410 (2005)
10. Kelly, J.M.: Base Isolation of Structures. Design Guidelines. Holmes Consulting Group Ltd., Wellington (2001)
11. Milani, G., Milani, F.: Stretch-stress behavior of elastomeric seismic isolators with different rubber materials. A numerical insight. Journal of Engineering Mechanics ASCE 138(5), 416–429 (2012a)
12. Milani, G., Milani, F.: Elastomeric seismic isolators behavior at different pads thickness. In: Pina, N., Kacprzyk, J. (eds.) Proc. 2nd International Conference on Simulation and Modeling Methodologies, Technologies and Applications, Rome, IT, July 28-31 (2012b)
13. Moon, B.Y., Kang, G.J., Kang, B.S., Kim, G.S., Kelly, J.M.: Mechanical properties of seismic isolation system with fiber-reinforced bearing of strip type. International Applied Mechanics 39(10), 1231–1239 (2003)
14. Mooney, M.: A theory of large elastic deformation. J. Appl. Physics 2, 582–592 (1940)
15. OPCM 3431: Ulteriori modifiche ed integrazioni all'OPCM 3274/ 03 20/03/2003. Primi elementi in materia di criteri generali per la classificazione sismica del territorio nazionale e di normative tecniche per le costruzioni in zona sismica (2005) (in Italian)
16. Qi, H.J., Joyce, K., Boyce, M.C.: Durometer hardness and the stress-strain behavior of elastomeric materials. Rubber Chemistry and Technology 72(2), 419–435 (2003)
17. Studebaker, M.L., Beatty, J.R.: The rubber compound and its composition. In: Eirich, F.R. (ed.) Science and Technology of Rubber. Academic Press, NY (1978)
18. Tobolsky, A.V., Mark, H.F.: Polymer Science and Materials, ch. 13. Wiley, New York (1971)
19. Tsai, H.S., Kelly, J.M.: Stiffness Analysis of Fiber-Reinforced Rectangular Seismic Isolators. Journal of Engineering Mechanics ASCE 128(4), 462–470 (2002)
20. Tsai, H.S., Lee, C.C.: Tilting stiffness of elastic layers bonded between rigid plates. International Journal of Solids and Structures 36(17), 2485–2505 (1999)